STEM CELLS TRANSLATIONAL MEDICINE®

TISSUE ENGINEERING AND REGENERATIVE MEDICINE

Functional Voltage-Gated Calcium Channels Are Present in Human Embryonic Stem Cell-Derived Retinal Pigment Epithelium

IINA KORKKA,[a] TAINA VIHERIÄLÄ,[a,b] KATI JUUTI-USITALO,[b] HANNELE UUSITALO-JÄRVINEN,[c,d] HELI SKOTTMAN,[b] JARI HYTTINEN,[a] SOILE NYMARK[a]

Key Words. Retinal pigment epithelium • Voltage-gated Ca^{2+} channels • Stem cells • Patch-clamp • Vascular endothelial growth factor • Phagocytosis

[a]Faculty of Biomedical Sciences and Engineering, BioMediTech, Tampere University of Technology, Tampere, Finland; [b]Faculty of Medicine and Life Sciences, BioMediTech, University of Tampere, Tampere, Finland; [c]Eye Centre, Tampere University Hospital, Tampere, Finland; [d]Faculty of Medicine and Life Sciences, Department of Ophthalmology, University of Tampere, Tampere, Finland

Correspondence: Soile Nymark, Ph.D., Arvo Ylpön katu 34, 33520 Tampere, Finland. Telephone: 358 40 849 0009; e-mail: soile.nymark@tut.fi

Received February 5, 2018; accepted for publication September 7, 2018; first published November 4, 2018.

http://dx.doi.org/10.1002/sctm.18-0026

ABSTRACT

Retinal pigment epithelium (RPE) performs important functions for the maintenance of photoreceptors and vision. Malfunctions within the RPE are implicated in several retinal diseases for which transplantations of stem cell-derived RPE are promising treatment options. Their success, however, is largely dependent on the functionality of the transplanted cells. This requires correct cellular physiology, which is highly influenced by the various ion channels of RPE, including voltage-gated Ca^{2+} (Ca_V) channels. This study investigated the localization and functionality of Ca_V channels in human embryonic stem cell (hESC)-derived RPE. Whole-cell patch-clamp recordings from these cells revealed slowly inactivating L-type currents comparable to freshly isolated mouse RPE. Some hESC-RPE cells also carried fast transient T-type resembling currents. These findings were confirmed by immunostainings from both hESC- and mouse RPE that showed the presence of the L-type Ca^{2+} channels $Ca_V1.2$ and $Ca_V1.3$ as well as the T-type Ca^{2+} channels $Ca_V3.1$ and $Ca_V3.2$. The localization of the major subtype, $Ca_V1.3$, changed during hESC-RPE maturation co-localizing with pericentrin to the base of the primary cilium before reaching more homogeneous membrane localization comparable to mouse RPE. Based on functional assessment, the L-type Ca^{2+} channels participated in the regulation of vascular endothelial growth factor secretion as well as in the phagocytosis of photoreceptor outer segments in hESC-RPE. Overall, this study demonstrates that a functional machinery of voltage-gated Ca^{2+} channels is present in mature hESC-RPE, which is promising for the success of transplantation therapies.
STEM CELLS TRANSLATIONAL MEDICINE *2019;8:179–193*

SIGNIFICANCE STATEMENT

Human stem cells provide a promising cell source for the replacement of diseased retinal pigment epithelium (RPE) in the eye, and several clinical trials with cell transplantations are ongoing. The success of these therapies is largely dependent on the correct functionality of the transplanted cells. Still, cellular ion channels, vital for the proper RPE physiology, are inadequately characterized in stem cell-derived RPE. The results of this study demonstrate the presence and functionality of voltage-gated Ca^{2+} channels in mature human embryonic stem cell-derived RPE similar to native RPE, and provide insight into their physiological relevance. This work is a significant contribution toward a more detailed functionality confirmation of stem cell-derived RPE.

INTRODUCTION

Retinal pigment epithelium (RPE) is a monolayer of polarized cells located in the back of the eye between the photoreceptors and the choroid, and forms a part of the blood-retinal-barrier [1]. As a barrier, RPE regulates the transport of nutrients and ions between the bloodstream and the subretinal space. In addition, RPE performs essential functions for vision such as phagocytosis, secretion, visual cycle, and light absorption (reviewed in [2]). RPE also plays a critical role in the pathogenesis of several degenerative eye diseases such as age-related macular degeneration (AMD) [3] that is the leading cause of vision loss and blindness among the elderly worldwide [4]. Stem cells provide potential for the development of transplantation therapies producing a limitless source of RPE cells for the treatment of AMD and other RPE-originated retinal dystrophies [5]. Remarkably, such therapies are already being subjected to clinical trials for AMD and Stargardt's macular dystrophy [6–21]

as well as to several preclinical trials [5, 22–28]. Stem cell-derived RPE has been demonstrated to resemble native tissue in many respects: it has been shown to have a proteome closely similar to the native counterpart [29], phagocytose photoreceptor outer segment (POS) fragments [27, 28, 30–32], secrete vascular endothelial growth factor (VEGF) [32–34], and participate in the functional visual cycle [35, 36]. However, much is still not understood about the genetic characteristics of stem cell-derived RPE [37] or its behavior after transplantation [38]. Furthermore, there is only limited information about the functionality of ion channels [33] and Ca^{2+} signaling [31, 39, 40] in stem cell-derived RPE. In particular, studies about the voltage-gated Ca^{2+} (Ca_V) channels in these cells are lacking.

The correct operation of Ca_V channels is required in order for the stem cell-derived RPE to perform its critical functions in therapeutic use, since many of the important RPE functions are related to changes in intracellular Ca^{2+} concentration [2]. L-type Ca^{2+} channels have been identified in cultured and native RPE [41–55], where they participate in the transport of ions and water [42] as well as the regulation of POS phagocytosis [41], VEGF secretion [43], and RPE differentiation [2]. On the other hand, the malfunctioning of L-type Ca^{2+} channels in RPE has been linked to the pathogenesis of certain degenerative eye diseases [45, 56]. Of the L-type Ca^{2+} channels, RPE has been shown to express the subtypes $Ca_V1.1$–1.3 [46] with several studies suggesting that subtype $Ca_V1.3$ is the primary contributor to RPE physiology [41, 43, 46, 50–55]. Of the T-type Ca^{2+} channels, RPE has been reported to express the subtypes $Ca_V3.1$ and $Ca_V3.3$, and it has been speculated that these channels participate in the regulation of VEGF secretion [46]. To date, α subtypes of the third subfamily $Ca_V2.x$ have not been detected in RPE [46]. It is, however, unclear whether this impressive machinery of Ca^{2+} channels is present in stem cell-derived RPE, and raises a question about the resemblance of human embryonic stem cell (hESC)-derived RPE to native RPE.

To address this issue, we investigated the functionality and localization profile of Ca_V channels in hESC-RPE. Here, we present our patch-clamp recordings that reveal slowly inactivating L-type currents in hESC-RPE that are similar to native RPE. In some hESC-RPE cells, fast transient currents that resemble T-type currents were also recorded. When compared with mouse tissue, there were similarities, as well as certain differences, in the localization of Ca_V channels in hESC-RPE. With regard to physiology, we show that L-type Ca^{2+} channels participate in POS phagocytosis and the regulation of VEGF secretion in hESC-RPE. Overall, our results suggest that a functional machinery of voltage-gated Ca^{2+} channels is present in hESC-RPE, and thus strengthen the potential of stem cell-derived RPE in transplantation therapies.

Materials and Methods

Culture of hESC-RPE

In this study, we used the previously derived hESC lines Regea08/023, Regea08/017, and Regea11/013 [57]. The undifferentiated hESCs were maintained, cultured, and spontaneously differentiated as described before [58]. After approximately 72–124 days of differentiation in the suspension culture, the pigmented areas of the floating aggregates were manually separated. The pigmented cell clusters were dissociated with TrypLE Select (Invitrogen, UK) and seeded onto Collagen IV (5 μg/cm^2, Sigma-Aldrich, St. Louis, MO) coated 24-well cell culture plates (Corning CellBIND; Corning, Inc., Corning, NY) with a density of 5.5×10^5 cells/cm^2. The cells were cultured for approximately 22–73 days, and cells from several independent differentiation batches were used for the study.

The cells were passaged with a density of 2.5×10^5 cells/cm^2 onto polyethylene terephthalate coated hanging culture inserts (pore size 1 μm, Merck Millipore) treated with Collagen IV (10 μg/cm^2, Sigma-Aldrich) or with Collagen IV and laminin (1.8 μg/cm^2, LN521, Biolamina, Sweden). The cultures became confluent in 5 days on inserts, after which they were further cultured until mature monolayers were obtained (days post-confluence presented in each figure legend). For single cell patch-clamp experiments, the cells were detached from the inserts with TrypLE Select and let to adhere on cover slips treated with poly-L-lysine (Sigma-Aldrich).

Isolation of Mouse RPE

We used C57BL/6 mice at the age of 8–12 weeks where the development and maturation of RPE had been completed [59]. The mice were euthanized by CO_2 inhalation and cervical dislocation. The eyes were then enucleated and bisected along the equator. The eyecups were sectioned in Ames' solution (Sigma-Aldrich) with 10 mM HEPES and pH adjusted to 7.4, and the retina was gently removed leaving the RPE firmly attached to the eyecup. To isolate the RPE cells for patch-clamp recordings, the eyecup was incubated at 37°C in 5% CO_2 either in TrypLE Select for 15 minutes or in a solution containing (in mM) 135 TeaCl, 5 KCl, 10 HEPES, 3 EDTA-KOH, 10 glucose, and 25 U/ml activated papain (Sigma-Aldrich) for 30 minutes. After this, the eyecups were washed in the HEPES buffered Ames' solution supplemented with 1% bovine serum albumin (BSA; Sigma-Aldrich). The RPE was collected by gentle trituration, stored at 37°C in 5% CO_2 in the RPE culture medium and measured within 6 hours.

Ethical Issues

Approval for research with human embryos was given by the National Authority for Medicolegal Affairs, Finland (Dnro 1426/32/300/05). A supportive statement was received from the Local Ethics Committee of the Pirkanmaa Hospital District, Finland to derive and expand hESC lines from surplus embryos, and to use these cell lines for research purposes (R05116). No new cell lines were derived in this study. The procedures carried out with C57BL/6 mice were in accordance with the ARVO Statement for the Use of Animals in Ophthalmic and Vision Research and the Finnish Animal Welfare Act 1986.

Patch-Clamp Recordings

Patch-clamp recordings were performed at room temperature (RT) on single hESC-RPE and mouse RPE cells. Ionic currents were recorded using the standard patch-clamp technique in whole-cell configuration. To minimize potassium currents, patch pipettes (resistance 4–8 MΩ) were filled with a cesium based internal solution containing (in mM) 83 $CsCH_3SO_3$, 25 CsCl, 5.5 EGTA, 0.5 $CaCl_2$, 4 ATP-Mg, 0.1 GTP-Na, 10 HEPES, and 5 NaCl; pH was adjusted to ~7.2 with CsOH and osmolarity was adjusted to ~290 mOsm with sucrose. The internal solution contained 2 mM lidocaine *N*-ethyl chloride (Sigma-Aldrich) to exclude the possibility of the measured fast transient currents being carried

by sodium [60]. The tissue was perfused with a control external solution containing (in mM): 120 NaCl, 5 TeaCl, 1.1 $CaCl_2$, 1.2 $MgCl_2$, 10 HEPES, 5 glucose, and 10 $BaCl_2$. pH was adjusted to 7.4 with NaOH and the osmolarity was set to ~305 mOsm with sucrose. In some experiments, the $BaCl_2$ concentration was decreased to 1 mM, and this was compensated by increasing the NaCl concentration to 130 mM. In the experiments that used Ca^{2+} channel modulators, the control bath solution contained L-type Ca^{2+} channel activator 10 μM (-)BayK8644 (Sigma-Aldrich) or L-type Ca^{2+} channel inhibitor 10 μM nifedipine (Sigma-Aldrich). The recordings were made in voltage-clamp mode using the Axopatch200B patch-clamp amplifier connected to an acquisition computer via AD/DA Digidata1440 (Molecular Devices, CA). Potentials were corrected for a 10 mV liquid junction potential during data analysis. Access resistance was <25 MΩ and membrane resistance was >300 MΩ. The membrane capacitance was 33 ± 5 pF (mean ± SEM, n = 9) for hESC-RPE cells and 23 ± 3 pF (mean ± SEM, n = 3) for mouse RPE cells. The depletion of the currents in hESC-RPE cells in whole-cell configuration was −11 ± 3% during 19 ± 5 minutes (mean ± SEM, n = 3) measured using a 50 ms voltage step from −100 to 10 mV. The measurements lasted for a shorter time than that of depletion. Current–voltage (IV)-curves were obtained from the peak value of the current at given voltages. Conductance (G) was calculated as $G = I/(V–V_R)$, where V_R is the reversal potential.

Indirect Immunofluorescence Staining

For immunofluorescence staining, hESC-RPE monolayers and mouse RPE eyecups were fixed for 15 minutes with 4% paraformaldehyde. The hESC-RPE monolayers and mouse RPE eyecup whole mount preparations were permeabilized by 15 minutes incubation in 0.1% Triton X-100 (Sigma-Aldrich) at RT. This was followed by incubation with 3% BSA in phosphate-buffered saline (PBS) (Sigma-Aldrich) at RT for 1 hour. Primary antibodies for $Ca_V1.1$, $Ca_V1.2$, $Ca_V1.3$, $Ca_V3.1$, $Ca_V3.2$, $Ca_V3.3$ (1:100; Alomone Labs, Jerusalem, Israel), cellular retinaldehyde-binding protein (CRALBP; 1:500; Abcam, UK), zonula occludens (ZO-1; 1:50; Life Technologies), claudin-3 (1:80; Thermo Fisher Scientific), ezrin (1:100; Abcam, UK), acetylated α-tubulin (1:1,000; Sigma-Aldrich), and pericentrin (PCNT; 1:200; Abcam, UK) were diluted in 3% BSA-PBS and incubated for 1 hour at RT. The samples were then washed four times with PBS, followed by 1 hour incubation at RT with the secondary antibodies donkey anti-rabbit or anti-mouse Alexa Fluor 488 and donkey anti-rabbit or anti-mouse Alexa Fluor 568 (1:200; Life Technologies) as well as goat anti-rabbit or anti-mouse Alexa Fluor 488 and goat anti-mouse Alexa Fluor 568 (1:200; Thermo Fisher Scientific) diluted in 3% BSA-PBS. Phalloidin was visualized using Phalloidin-Atto 633 (1:100; Sigma-Aldrich), an Alexa Fluor 568 conjugate (1:400; Sigma-Aldrich) or an Alexa Fluor 647 conjugate (1:50; Life Technologies). The washes with PBS were repeated and the nuclei were stained with the 4′,6-diamidino-2-phenylidole included in the mounting medium (Life Technologies).

For paraffin embedded vertical sections, the hESC-RPE monolayers and mouse eyecups with retina attached were infused in paraffin blocks and cut into 7 μm vertical sections with a Leica SM2000 R or Leica SM2010 R sliding microtome (Leica Biosystems). The sections were then attached on glass coverslides by 1 hour incubation at 60°C. The samples were deparaffinized and hydrolyzed using xylene and ethanol series. Antigen retrieval was carried out by microwaving the samples in 10 mM sodium citrate in 0.05% Tween20 (Sigma Aldrich). The samples were blocked using 10% donkey serum and 5% BSA in tris-buffered saline (TBS) for 1 hour at 37°C. After this, they were washed twice in 0.02% Tween20-TBS. The Ca_V primary antibodies listed above, as well as Na^+/K^+-ATPase (1:200; Abcam) and Bestrophin-1 (1:500; Lagen laboratories) were diluted in 1% BSA-TBS and incubated overnight at 4°C. The samples were then washed twice with 0.02% Tween20-TBS. The secondary antibodies introduced above were diluted with 1% BSA-TBS and incubated for 1 hour at RT, followed by two washes and mounting as described above.

Confocal Microscopy and Image Processing

Confocal microscopy was performed with a Zeiss LSM780 or LSM700 laser scanning confocal microscope (LSCM) on an inverted Zeiss Cell Observer microscope (Zeiss, Jena, Germany) and Plan-Apochromat ×63/1.4 oil immersion objective. Voxel size was set to $x = y$ = 66 nm and z = 100–200 nm and image size to 512 × 512 or 1,024 × 1,024 pixels. Reflection imaging was conducted by collecting light from the 488 nm laser line by using 20/80 dichroic beam splitter and 480–492 nm emission window at the photomultiplier tube detector. The images were saved in czi-format and processed with ImageJ [61], adjusting only brightness and contrast, and panels were assembled using Adobe Photoshop CS6 (Adobe Systems, San Jose).

Pulse-Chase Phagocytosis Assay

Mature hESC-RPE monolayers on culture inserts were preincubated for 24 hours at 37°C in the control medium or in the presence of the L-type Ca_V modulators 10 μM (-)BayK8644, or 10 μM nifedipine, or T-type Ca_V inhibitor 5 μM ML218 (Sigma-Aldrich). For phagocytosis assay, POS fragments were isolated and purified from fresh porcine eyes obtained from a local slaughterhouse as described before [58, 62]. The POS particles were suspended to 10% fetal bovine serum (FBS) containing medium in control or in one of the drug containing conditions. In the pulse stage, equal amounts of POS containing media were added on the apical sides of the hESC-RPE inserts and incubated for 30 minutes at 37°C. For the chase stage, the media were changed back to 10% FBS medium with or without the drugs, and the hESC-RPE inserts were further incubated for 2 hours at 37°C. After this, the samples were fixed and stained as described above using the primary antibodies opsin (1:200; Sigma Aldrich) and ZO-1. The samples were imaged using the Zeiss LSM780 LSCM as described above but by imaging large random fields. The number of bound and internalized POS particles that were larger than 1 μm in diameter, were counted from maximum intensity projection images after performing Gaussian blur using ImageJ. The assay was performed with three inserts in each condition and data from 5 to 6 images from each of the three inserts was pooled together resulting in n = 15–16.

Enzyme-Linked Immunosorbent Assay for VEGF Secretion

Secretion of VEGF by mature hESC-RPE was assessed with a commercially available human VEGF Quantikine enzyme-linked immunosorbent assay (ELISA) kit (R&D Systems, MN) according to the manufacturer's instructions. Briefly, the polarized VEGF secretion in control conditions was studied by collecting medium samples separately from the apical and basolateral sides of the

insert after 24 hours incubation with three replicates. To test the effect of Ca_V channel modulators on VEGF secretion, we measured the total VEGF concentration secreted through both apical and basolateral cell membranes. The inserts were incubated 24 hours in different pharmacological conditions: in 1% FBS medium in control conditions, or in this medium together with 10 μM (-)BayK8644, 10 μM nifedipine or 5 μM ML218 with eight to nine replicates. The VEGF concentration from the collected medium samples was normalized to the number of cells based on cell counting under the Zeiss LSM780 LSCM using ×20 or ×63 objective.

Statistical Analysis

The data is stated as mean ± SEM (*n*, *p*), where *n* refers to the number of samples used to generate the data set and *p* refers to statistical significance. The data was tested for normality using the Shapiro–Wilk normality test. Some of the data sets did not meet the normality criteria. Thus, a pair-wise comparison of the test conditions to control condition was conducted using nonparametric Mann-Whitney *U* test to confirm the possible statistical significance between the experimental conditions.

RESULTS

Currents Through Voltage-Gated Ca^{2+} Channels in hESC-RPE

In control conditions with 10 mM extracellular Ba^{2+}, whole-cell voltage clamp recordings revealed voltage-gated currents in single hESC-RPE cells (Fig. 1A) dissociated from a mature RPE monolayer (Fig. 1B). In response to a 50 ms voltage pulse from −80 to 60 mV in 10 mV steps, nine cells showed slowly or non-inactivating currents (Fig. 1C). Based on the normalized and averaged IV-curve (*n* = 9), the current activated at low potentials reaching maximum at 10 mV (Fig. 1D). The normalized and averaged GV-curve showed half maximum conductance at −7 ± 3 mV (*n* = 9) (Fig. 1E). Typical to L-type Ca^{2+} channels [47, 48], diminishing the Ba^{2+} content from 10 to 1 mM decreased the maximum current density from 2.4 ± 0.5 $pA{\cdot}pF^{-1}$ (*n* = 9) to 1.3 ± 0.3 $pA{\cdot}pF^{-1}$ (*n* = 7) (Fig. 1F). In addition, three cells showed fast transient currents (Fig. 1G) with inactivation time constant 6 ± 1 ms (*n* = 3). The current pattern indicated that hESC-RPE is likely to express both slowly inactivating L-type currents and fast inactivating T-type resembling currents. However, a detailed characterization of the fast inactivating currents was not possible as will be discussed later.

The Effects of L-Type Ca^{2+} Channel Activator and Inhibitor

The effects of (-)BayK8644 and nifedipine, well-characterized activator and inhibitor of the L-type Ca^{2+} channels, were tested for the slowly inactivating currents. These currents were increased by 10 μM (-)BayK8644 (Fig. 2A, 2C) and decreased by 10 μM nifedipine (Fig. 2B, 2D). Comparison with the control current at maximum amplitude revealed that the slowly inactivating current increased after (-)BayK8644 application by 80 ± 9% (*n* = 3, $p < .05$) (Fig. 2E) and decreased after nifedipine application by 56 ± 5% (*n* = 4, $p < .05$) (Fig. 2F). Both effects were statistically significant. These recordings confirm that the slowly inactivating currents were carried by the L-type Ca^{2+} channels.

Localization of Voltage-Gated Ca^{2+} Channels in hESC-RPE

To evaluate the localization of the Ca_V channels detected in the patch-clamp measurements in hESC-RPE, we performed antibody labeling against the L-type Ca^{2+} channels $Ca_V1.1$-$Ca_V1.3$ and the T-type Ca^{2+} channels $Ca_V3.1$-$Ca_V3.3$, together with markers for actin cytoskeleton, RPE maturity, and polarization. The hESC-RPE showed a typical expression of CRALBP (Fig. 3A) and Na^+/K^+-ATPase (Fig. 3F) on the apical side of the monolayer, as well as Bestrophin-1 primarily on the basolateral side (Fig. 3F). Zonula occludens (ZO-1) (Fig. 3B) and claudin-3 (Fig. 3C) co-localized on the cell–cell junctions with the circumferential bands of actin (phalloidin), characteristic to mature RPE [63]. This data, together with the TER value of over 200 Ω cm^2, strong pigmentation and cobblestone morphology (see Fig. 1B), indicate the maturity and polarization of our hESC-RPE.

The most prominent staining in hESC-RPE monolayers was detected for the subtypes $Ca_V1.3$ and $Ca_V3.1$, both localizing strongly at the apical membrane (Fig. 3D, 3E). Staining of these subtypes together with RPE microvilli marker ezrin revealed the localization of $Ca_V1.3$ right below the microvilli (Supporting Information Fig. S1A) and $Ca_V3.1$ at the microvilli (Supporting Information Fig. S1B). Since pigmentation hinders the visualization of the basolateral side (see yz confocal sections in Fig. 3), we performed immunostainings on paraffin embedded vertical sections of the hESC-RPE. This confirmed the apical localization of the subtypes $Ca_V1.3$ (Fig. 3H) and $Ca_V3.1$ (Fig. 3I) and revealed a pronounced basolateral localization of $Ca_V1.3$ (Fig. 3H). Furthermore, in hESC-RPE, we observed basolateral localization of $Ca_V1.2$ (Fig. 3G), and basolateral and junctional localization of $Ca_V3.2$ (Fig. 3J). The $Ca_V1.1$ and $Ca_V3.3$ subtypes were not detected (data not shown).

Voltage-Gated Ca^{2+} Channels in Mouse RPE

To compare the currents through voltage-gated Ca^{2+} channels in hESC-RPE with native tissue, patch-clamp recordings were performed from the cells of freshly isolated mouse RPE (Fig. 4). An investigation of currents in whole-cell configuration as a response to series of depolarizing voltage steps from −80 to +60 mV revealed slowly inactivating currents in the recordings (Fig. 4A). The currents activated at low potentials reaching the maximum at 20 mV in the normalized and averaged IV-curve (*n* = 4) (Fig. 4B). The half maximum conductance was reached at −6 ± 3 mV (*n* = 4) based on the normalized and averaged GV-curve (Fig. 4C). The maximum current density of the slowly inactivating current was 2.3 ± 0.6 $pA{\cdot}pF^{-1}$ (*n* = 4). Thus, the current characteristics of the voltage-gated Ca^{2+} channels in mouse RPE were comparable to those we identified in hESC-RPE.

Antibody labeling, similar to hESC-RPE, was performed on mouse RPE-eyecup whole mount preparations (Fig. 4D, 4E, Supporting Information Fig. S1C, S1D) and vertical sections of paraffin embedded eyecups (Fig. 4F–4I). The channel localization in mouse RPE followed similar characteristics as in hESC-RPE with the exception that the apically localized $Ca_V3.1$ was also detected at the basolateral side in mouse RPE (Fig. 4H). Furthermore, it is worth pointing out, that the uniform apical staining profile of $Ca_V1.3$ observed in hESC-RPE (Fig. 3D, 3H, Supporting Information Fig. S1A) was especially strongly detected in mouse RPE (Fig. 4D, 4G, Supporting Information Fig. S1C).

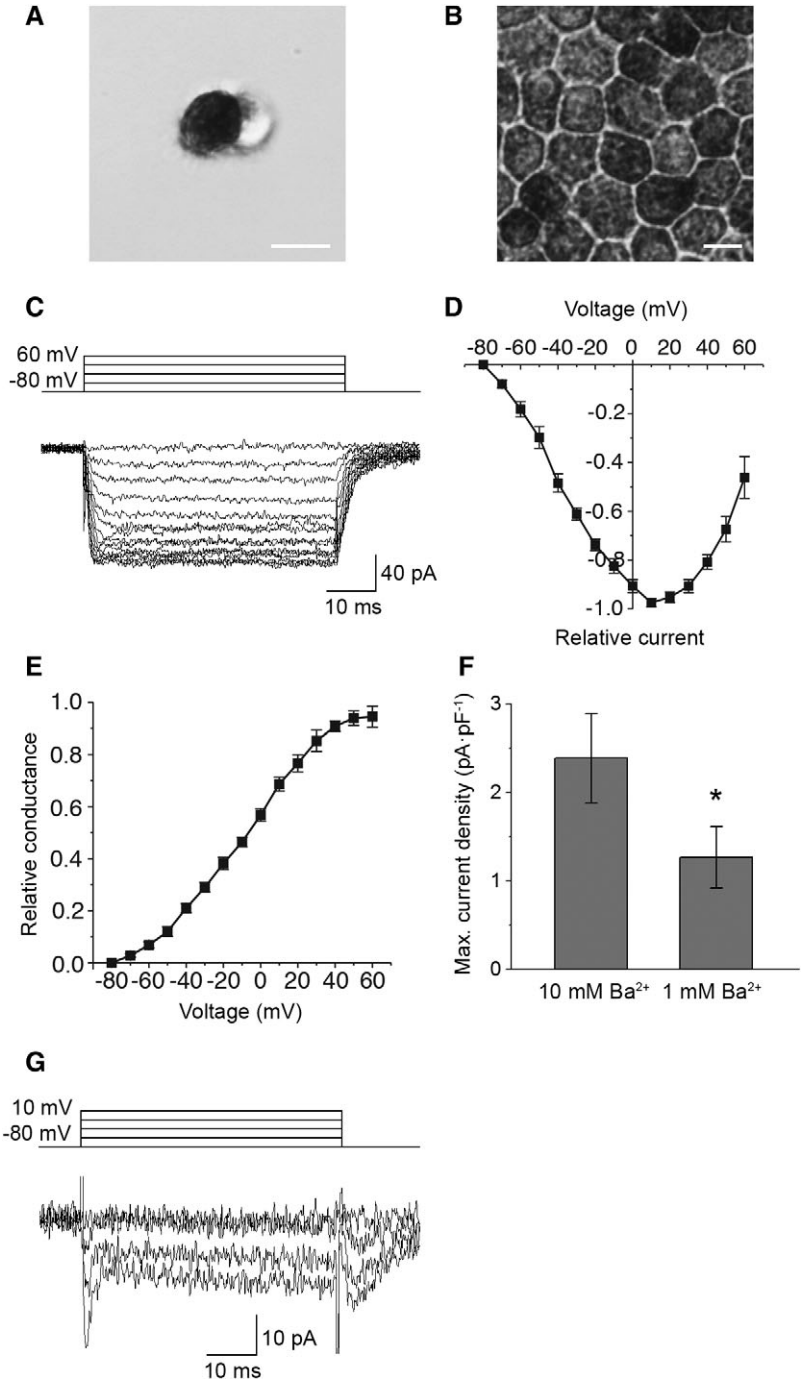

Figure 1. Voltage-gated currents in hESC-RPE. Examples of bright-field microscopy images of **(A)** a single hESC-RPE cell showing pigmented apical and non-pigmented basal sides and **(B)** a mature hESC-RPE monolayer with representative RPE morphology, scale bars 10 μm. Whole-cell voltage clamp recordings were carried out from single hESC-RPE cells. **(C):** A typical example of the slowly inactivating current elicited by 50 ms voltage steps from −80 to +60 mV in 10 mV increments. Normalized and averaged **(D)** IV-curve and **(E)** GV-curve of the slowly inactivating current (mean ± SEM, n = 9, cell lines 08/017 and 08/023, days post-confluence 73–128). **(F):** Averaged maximum current densities (obtained at 10 mV) of the slowly inactivating current in 10 mM Ba^{2+} (n = 9) and in 1 mM Ba^{2+} (n = 7, cell lines 08/017 and 08/023, days post-confluence 109–127). The difference in the current densities was statistically significant. **(G):** A typical example of the fast inactivating current elicited by 50 ms voltage steps from −80 to +10 mV in 10 mV increments (cell line 08/023, days post-confluence 109). *Statistically significant difference with $p < .05$.

VEGF Secretion in hESC-RPE

In hESC-RPE, characteristic to RPE physiology, VEGF secretion was polarized. Consistent with this, we found that the amount of VEGF secreted after a 24 hour incubation in control conditions was 588 ± 37 pg/10^5 cells to the apical side and 1,290 ± 38 pg/10^5 cells to the basolateral side (n = 3). Since the L-type Ca^{2+} channels have been reported to play an important role in VEGF secretion [43], we investigated the effect of their

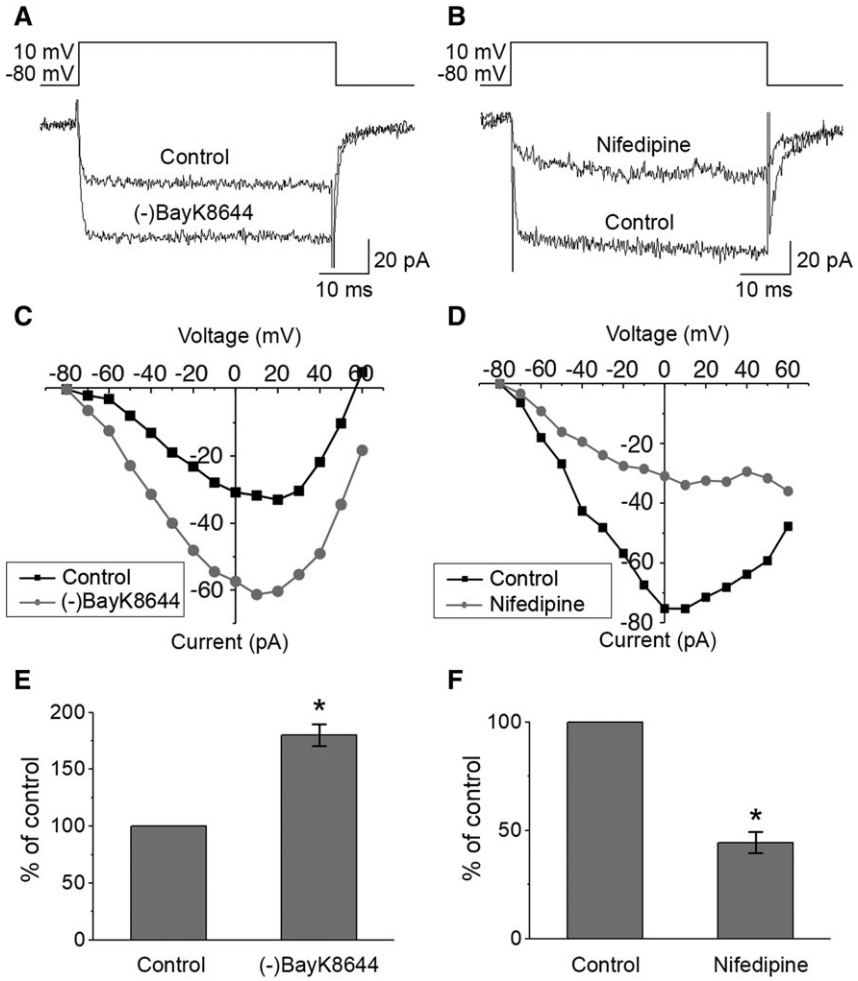

Figure 2. Responses of the currents to Ca^{2+} channel modulators. Whole-cell measurements of currents as responses to voltage pulses from −80 to +60 mV in 10 mV increments for 50 ms duration were performed before and after the application of the specific drugs. Examples of the effects of **(A)** L-type Ca^{2+} channel activator 10 μM (-)BayK8644 and **(B)** L-type Ca^{2+} channel inhibitor 10 μM nifedipine on Ba^{2+} currents in hESC-RPE and **(C, D)** the corresponding IV-curves, respectively. Changes in maximum current amplitudes presented as percentages from control conditions (mean ± SEM) show that both **(E)** activation with (-)BayK8644 (n = 3, cell line 08/017, days post-confluence 73–74) and **(F)** inhibition with nifedipine (n = 4, cell line 08/017, days post-confluence 73–99) resulted in statistically significant changes in the recorded currents. *Statistically significant difference with $p < .05$.

pharmacological modulation on the total amount of secreted VEGF in hESC-RPE. We followed the apical and basal secretion concurrently (Fig. 5) thus addressing the role of both apically and basally localized Ca^{2+} channels in the overall secretion. In control conditions, the total VEGF concentration in the medium after the 24 hour incubation was 1,950 ± 70 pg/10^5 cells (n = 9). Manipulation of the L-type Ca^{2+} channel activity directly affected the VEGF secretion as the activator (-)BayK8644 increased the secretion by 24 ± 9% (n = 9, $p < .05$) and the inhibitor nifedipine decreased the secretion by 19 ± 9% (n = 8, $p < .05$). Both effects were statistically significant. However, inhibition of the T-type channels by ML218 had little effect on the VEGF secretion (8 ± 14% increase, n = 8, $p > .05$).

Voltage-Gated Ca^{2+} Channels Regulate POS Phagocytosis in hESC-RPE

Previous studies indicate that L-type Ca^{2+} channels participate in the regulation of phagocytosis in RPE [41, 64]. Thus, we investigated the role of Ca_V channels in POS phagocytosis in hESC-RPE by pharmacologically modulating these channels during our phagocytosis assay. These experiments and subsequent labeling with opsin and ZO-1 showed a reduction in the total number of bound and internalized POS particles in the presence of either L-type channel activator or inhibitor, but an increase in the particle number in the presence of T-type channel inhibitor (Fig. 6). More specifically, the median value of POS particles in a randomly taken confocal image field decreased from the control conditions (n = 16, Fig. 6A, 6E) by 30% when the L-type channels were activated by (-)BayK8644 (n = 16, $p < .001$, Fig. 6B, 6E). A higher decrease of 62% occurred when the L-type Ca^{2+} channels were inhibited by nifedipine (n = 15, $p < .001$, Fig. 6C, 6E). Interestingly, we found that T-type Ca^{2+} channel inhibitor ML218 (Fig. 6D, 6E) increased the number of POS particles by 32% (n = 16, $p < .05$). All the effects were statistically significant.

Localization of $Ca_V1.3$ During hESC-RPE Maturation

It is well established that protein expression and localization change during RPE maturation [65]. We addressed this considering

the localization of the primary Ca_V channel subtype, $Ca_V1.3$, during hESC-RPE maturation. We immunolabeled $Ca_V1.3$ together with pericentrin (PCNT), a protein localized in the centrosomes at the base of the primary cilia, that have been recently shown to be important for RPE maturation [66, 67]. Figure 7 shows how the localization of these proteins changed remarkably during maturation. Fusiform hESC-RPE cells on the first day post-confluence (Supporting Information Fig. S2A) expressed $Ca_V1.3$ throughout the cell (Fig. 7A), and PCNT appeared as distinct puncta on the apical side. After 6 days post-confluence, the cells gained more epithelioid morphology (Supporting Information Fig. S2B) and $Ca_V1.3$ started to localize also to the apical and basal RPE cell membranes with brighter puncta forming on the apical side (Fig. 7B). Interestingly, these puncta showed co-localization with PCNT. The hESC-RPE cells obtained cobblestone morphology around 31 days post-confluence (Supporting Information Fig. S2C), and from this time point onwards, $Ca_V1.3$ was present more

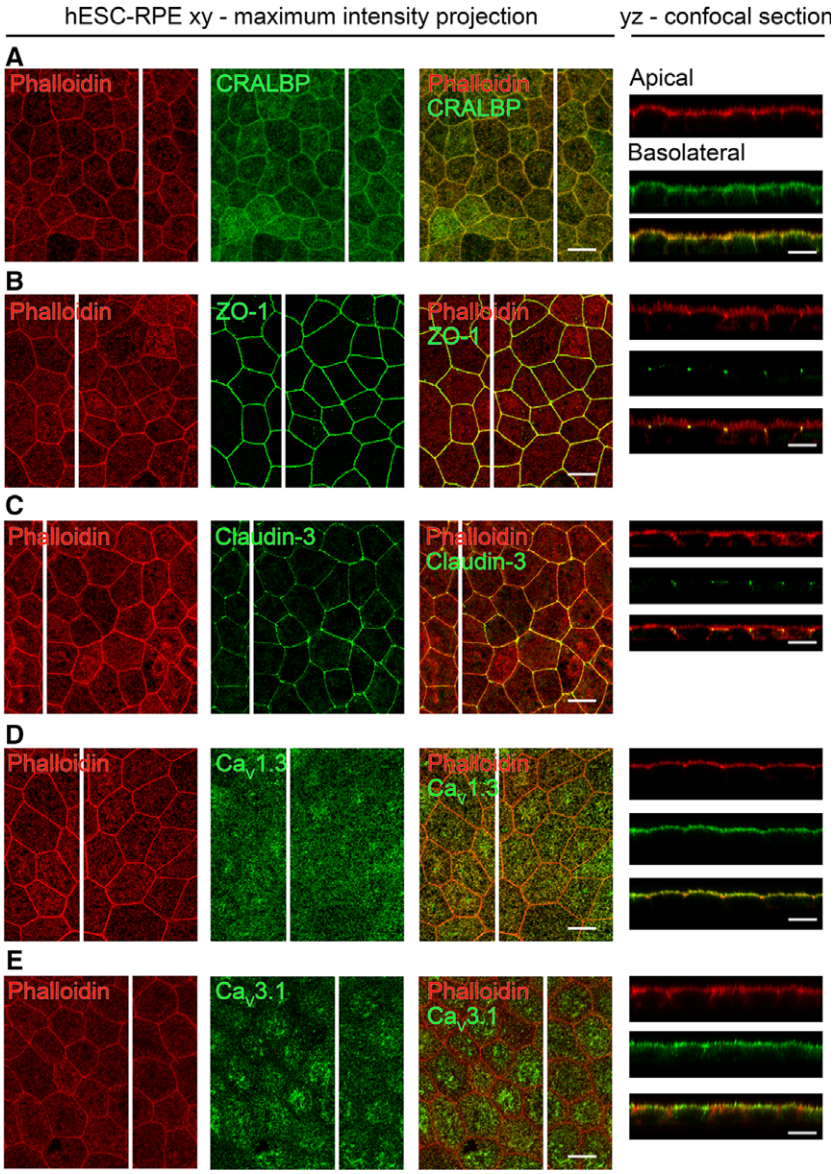

Figure 3. Localization of Ca_V channels in hESC-RPE. Immunostainings of RPE monolayers with xy-maximum intensity projections and yz-confocal sections (apical side upwards, localization of the section highlighted with a white bar). Actin cytoskeleton (phalloidin, red) labeled together with **(A)** RPE marker CRALBP (green, cell line 08/017, days post-confluence 91), **(B)** tight junction markers ZO-1, (green, cell line 08/017, days post-confluence 74) and **(C)** claudin-3 (green, cell line 08/017, days post-confluence 91), **(D)** L-type Ca^{2+} channel $Ca_V1.3$ (green, cell line 08/017, days post-confluence 109), and **(E)** T-type Ca^{2+} channel $Ca_V3.1$ (green, cell line 08/023, days post-confluence 66). Immunostainings of paraffin embedded hESC-RPE vertical sections with xy-maximum intensity projections (apical side upwards). **(F):** Cell polarization markers Na^+/K^+-ATPase (red) and Bestrophin-1 (green, cell line 08/023, days post-confluence 91). Cell nuclei (DAPI, blue) together with L-type Ca^{2+} channels **(G)** $Ca_V1.2$ (green, cell line 08/017, days post-confluence 84) and **(H)** $Ca_V1.3$ (green, cell line 08/023, days post-confluence 91), and T-type Ca^{2+} channels **(I)** $Ca_V3.1$ (green, cell line 08/017, days post-confluence 84) and **(J)** $Ca_V3.2$ (green, cell line 08/017, days post-confluence 84). Scale bars 10 µm. Abbreviations: Ca_V, voltage-gated Ca^{2+} channel; CRALBP, cellular retinaldehyde-binding protein; ZO-1, Zonula occludens; DAPI, 4′,6-diamidino-2-phenylidole; hESC, human embryonic stem cell; RPE, retinal pigment epithelium.

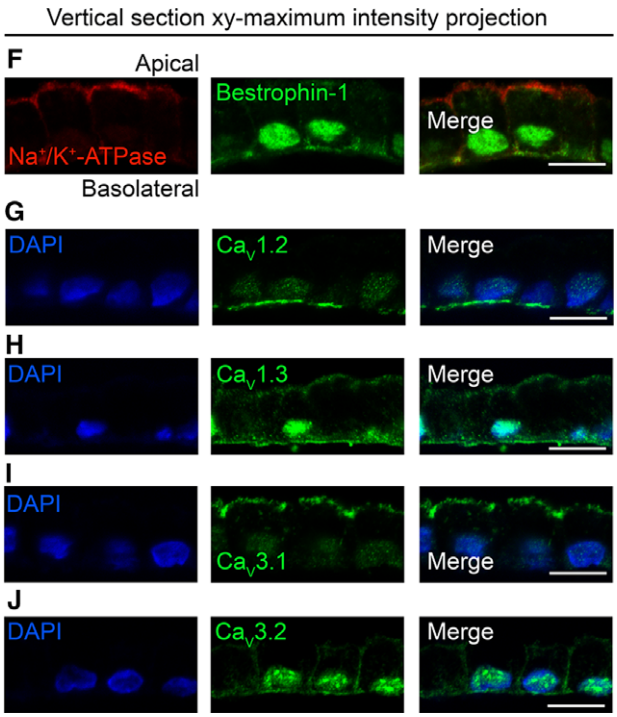

Figure 3. (Continued)

strongly on the apical and basolateral cell membranes (Fig. 7C). The apical side puncta were pronounced and appeared as one distinct cluster per cell co-localizing strongly with PCNT (Fig. 7C). Immunolabeling $Ca_V1.3$ with acetylated α-tubulin (Fig. 7E) showed the localization of $Ca_V1.3$ near the base of the primary cilia. With increasing maturation, the apical staining of $Ca_V1.3$ became more prominent and more homogeneous, while basolateral staining started to be difficult to detect due to increased pigmentation. At 84 days post-confluence (Fig. 7D), fairly uniform apical localization of $Ca_V1.3$ was present in hESC-RPE, although the puncta, co-localizing with PCNT, could still be distinguished. At this time point, PCNT localized near the apical centers of the cobblestone hESC-RPE cells (Fig. 7D, Supporting Information Fig. S2D), characteristic to mature RPE [67]. This data suggest that with increasing maturation, hESC-RPE started to gain the homogeneous apical localization of $Ca_V1.3$ detected in mouse RPE (Fig. 4D).

Discussion

Stem cell-derived RPE provides great potential for novel cell transplantation therapies and research has already proceeded to clinical trials [6–21]. Essential for the success of these therapies, stem cell-derived RPE has been shown to perform several key RPE functions [27–36]. However, the functionality of the ion channels and specifically the voltage-gated Ca^{2+} channels in these cells remain poorly known, even though many of the critical RPE functions are related to Ca^{2+} activity. This raises the question whether the stem cell-derived RPE destined for clinical purposes sufficiently resembles its native counterpart, and can thus replace the functions of lost cells. The present study addressed this issue by investigating the Ca_V channels in hESC-RPE. Using patch-clamp recordings and immunostainings, we showed the presence of functional L-type Ca^{2+} channels in hESC-RPE that are comparable to native mouse RPE.

In our study, two current types were detected, the slowly inactivating current and the fast inactivating current. We confirmed that the main current type, the slowly inactivating current, results from the activity of L-type Ca^{2+} channels since the current responses and IV-curves in this study resembled the previous recordings of L-type currents from various types of native RPE [43, 46–48]. Moreover, the sensitivity of the current to the L-type Ca^{2+} channel activator (-)BayK8644 [45–50, 53] and the inhibitor nifedipine [43, 44, 47, 48, 51] further indicated the presence of L-type currents in our measurements. The recorded current is likely to be carried primarily through $Ca_V1.3$ channels. This conclusion is based on the voltage-dependent activation of the currents at rather negative potentials [68], shape of the IV-curve characteristic to the $Ca_V1.3$ subtype [43, 46, 55], and slow inactivation of the current. It is still likely that $Ca_V1.2$ channels contribute to the recorded current as well, since our immunostainings confirmed the presence of both of the L-type Ca^{2+} channels, $Ca_V1.2$ and $Ca_V1.3$, in hESC-RPE. To date, $Ca_V1.3$ subtype has been reported to only localize basolaterally in murine [54] and porcine [55] RPE. Our data showed that both hESC- and mouse RPE express the $Ca_V1.3$ subtype also on the apical cell membrane, in addition to the basolateral membrane.

It is worth noting that patch-clamp recordings from primary RPE cultures show differences in L-type current characteristics when compared with our recordings from hESC-RPE [43, 45, 49, 50, 53], especially regarding the more negative activation threshold and the weaker slope of activation present in our study. The reason for this remains to be investigated, but it may be related to differences in phosphorylation, splicing variants, or the composition of the accessory subunits [69, 70]. Yet, the contribution of other Ca^{2+} conducting channels on the currents recorded in this study for hESC-RPE and native mouse RPE cannot be excluded. Several Ca^{2+}-conducting channels, such as store-operated Orai channels [71] and transient receptor potential (TRP) channels [41, 72–74], have important roles in the physiology of RPE. Relevant for this study, TRP channels are involved in the phagocytosis [41] and VEGF secretion [73]. In addition to these other Ca^{2+}-conductivities, the effect of cell dissociation to patch-clamp recordings needs to be taken into account. Cell–cell junctions break down in cell dissociation causing epithelial cells to lose their polarity, which compromises their normal ability to express and recycle proteins. This has a strong influence on the endocytotic processes that are important for the internalization of ion channels, regulating their numbers in the cell membrane [75]. Therefore, after cell dissociation, ion channels can be re-distributed to the intracellular compartments and those currents will thus be absent from the patch-clamp recordings.

In addition to L-type currents, our patch-clamp recordings revealed the presence of fast transient currents in hESC-RPE. The kinetics of these currents were comparable to those previously reported for the T-type Ca^{2+} channels in cultured human RPE [46], although faster than typically reported for other cell types (reviewed in [76]). Similar to the findings of the previous study [46], the fast transient currents were almost exclusively recorded in combination with the slowly inactivating current, which hindered their further analysis. In addition, TTX-sensitive currents can also contribute to the fast transient conductance

[60, 77] and make this current component extremely difficult to investigate. In immunostainings, we observed $Ca_V3.1$ and $Ca_V3.2$ in both hESC- and mouse RPE. $Ca_V3.1$ was localized apically at the microvilli in the both studied RPE cell types, while it was found also at the basolateral cell membrane in mouse RPE.

VEGF has a role in angiogenesis and vascular permeability, and therefore anti-VEGF agents are commonly used in the treatment of AMD [78]. In healthy RPE, VEGF secretion occurs in a polarized manner with significantly more pronounced secretion from the basal side [79, 80], as we showed here for hESC-RPE. This secretion is regulated by several factors including hyperosmolarity [81], hyperthermia [82], oxidative stress [83], and heat-sensitive TRPV channels [73]. Particularly relevant for this study, modulating the L-type Ca^{2+} channel activity has been shown to directly correlate with the VEGF secretion level [43]. Our ELISA results indicated similar behavior as the activator (-)BayK8644 increased the VEGF secretion and the inhibitor nifedipine decreased the VEGF secretion. This demonstrates that the L-type Ca^{2+} channels participate in the regulation of VEGF secretion in hESC-RPE. However, it is worth

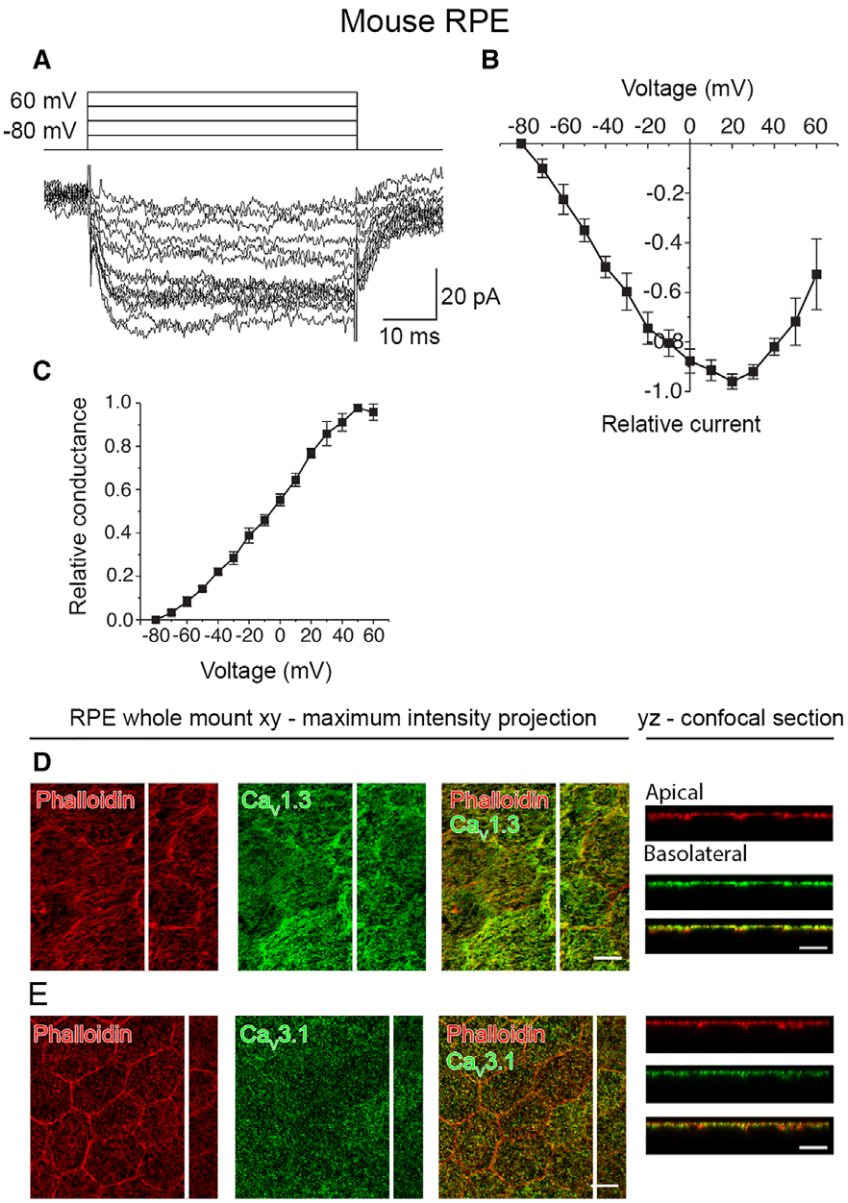

Figure 4. Ca_V channels in mouse RPE. **(A):** An example of the slowly inactivating L-type current measured in whole-cell configuration and elicited by 50 ms voltage steps from −80 to +60 mV in 10 mV increments. **(B):** Normalized and averaged IV-curve of the L-type current (mean ± SEM, n = 4). **(C):** Normalized and averaged GV-curve of the L-type current (mean ± SEM, n = 4). Localization of the Ca_V channels assessed by immunostainings of mouse RPE-eyecup whole mount preparations. Confocal images show the xy-maximum intensity projections and yz-confocal sections of the samples (apical side upwards, localization of the section highlighted with a white bar). Actin cytoskeleton (phalloidin, red) together with **(D)** L-type Ca^{2+} channel $Ca_V1.3$ (green), and **(E)** T-type Ca^{2+} channel $Ca_V3.1$ (green). Immunostainings of paraffin embedded vertical sections of mouse eyecups shown as xy-maximum intensity projections (apical side upwards). BF images together with L-type Ca^{2+} channels **(F)** $Ca_V1.2$ (green) and **(G)** $Ca_V1.3$ (green), and T-type Ca^{2+} channels **(H)** $Ca_V3.1$ (green) and **(I)** $Ca_V3.2$ (green). Scale bars 10 μm. Abbreviations: Ca_V, voltage-gated Ca^{2+} channel; BF, bright-field; RPE, retinal pigment epithelium.

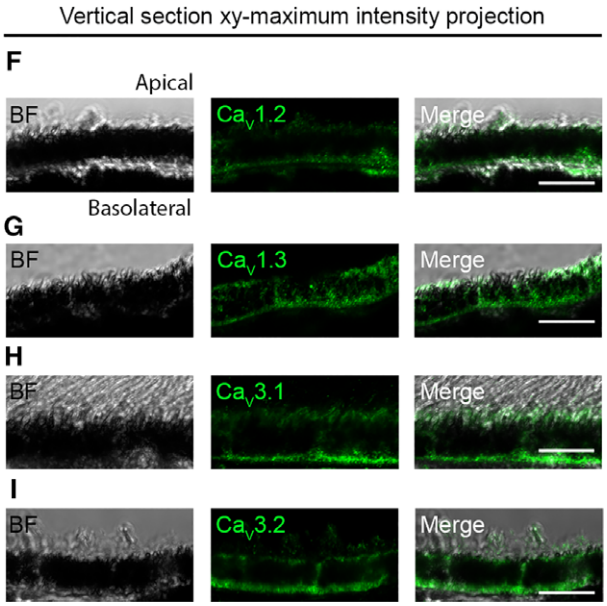

Figure 4. (Continued)

noting that the cell culture insert membrane with randomly spaced 1 μm holes may hinder both the diffusion of the drug to the basolateral cell membrane and the secretion of VEGF to the medium. Since the VEGF secretion is more pronounced in the basolateral side of the RPE, the structural constraints from the insert may lower the effect of pharmacological Ca^{2+} channel modulation on VEGF secretion.

Photoreceptor renewal is a critical task for RPE to maintain vision [2], and insufficient phagocytosis often leads to retinal diseases [84, 85]. Several ion channels, including the L-type Ca^{2+} channels, are known to have regulatory roles in phagocytosis in RPE [41, 64]. We found that in hESC-RPE, in line with the previous studies [64], inhibition of the L-type Ca^{2+} channels by nifedipine decreased the phagocytosis remarkably. On the other hand, activation of these channels by (-)BayK8644 also decreased the number of phagocytosed POS particles, although to a lesser extent. Interestingly, it was reported that in primary porcine RPE, the activation of L-type Ca^{2+} channels had no effect on phagocytosis, and this was suggested to be a consequence of the regulatory effect of bestrophin-1 setting a limit to L-type Ca^{2+} channel activity [41]. When comparing these results to our data, we want to point out that we used a pulse-chase POS phagocytosis assay, while Müller et al. [41] used an assay with continuous POS supply to the RPE cells that may lead to distinct outcomes. Moreover, it is possible that bestrophin-1 expression levels are much lower in hESC-RPE compared to primary porcine RPE [41] thus diminishing the regulatory effect of bestrophin-1 on L-type Ca^{2+} channels in our cells. Besides, the influence of Ca^{2+} in phagocytosis can also be inhibitory: increase in intracellular Ca^{2+} and subsequent activation of protein kinase C has been shown to reduce POS ingestion [86]. These observations indicate that the role for the L-type Ca^{2+} channels in the regulation of POS phagocytosis is a complex process (see also [41, 64]) and may include negative feedback mechanisms, especially after prolonged channel activation. Furthermore, it is known that these channels participate in the regulation of phagocytosis in concert with other ion channels including Ca^{2+}-dependent K^+ channels, bestrophin-1, TRPV [41], and most likely also the T-type Ca^{2+} channels. Our observation about the increased number of bound or ingested POS particles following T-type Ca^{2+} channel inhibition is similar to the effect of bestrophin-1 inhibition [41]. Analogous to bestrophin-1 [87], T-type Ca^{2+} channels are indicated to interact with the β subunits of the L-type Ca^{2+} channels [88]. This implies a possible role for the T-type channels to inhibit L-type channels through their interaction with β subunits. Taken together, these data demonstrate a need for further studies in elucidating the concerted functioning of Ca^{2+} conducting channels in the regulation of phagocytosis.

Regardless of the close resemblance between stem cell-derived and native RPE demonstrated for their proteome [29], capability of phagocytosis [27, 28, 30–32], VEGF secretion [32–34], and visual cycle [35, 36], many important differences have also been reported. These include a lower efficiency in the phagocytosis of POSs [89] as well as differences in growth factor secretion [90] and expression of adhesion junction and membrane transport genes [37]. We used mouse RPE as the native counterpart for hESC-RPE in our studies due to unavailability of live human RPE tissue. Previous work on gene and protein expression profiles of human and mouse RPE show high similarity regarding general biological functions, canonical pathways, and molecular networks [91, 92]. However, there are important species-specific differences between human and mouse RPE. These include immune regulation genes and genes related to the development of AMD and Usher syndrome [92] as well as the well-known anatomical differences such as the absence of macula in the mouse and differences in rod and cone types and distributions.

We studied the functionality of Ca_V channels in mature hESC-RPE where the localization of the primary Ca_V channel subtype, $Ca_V1.3$, started to resemble native RPE. During maturation, we observed significant changes in $Ca_V1.3$ localization in hESC-RPE implying that ion channels can be highly sensitive to the level of tissue maturity. This has been previously suggested at least for Bestrophin-1 in RPE [32, 93]. We

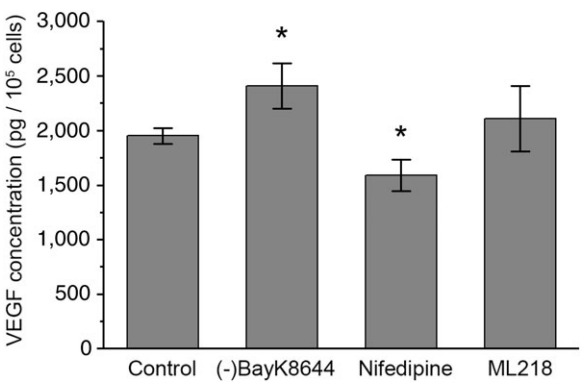

Figure 5. VEGF secretion from hESC-RPE. Total concentrations of VEGF secreted by the hESC-RPE after 24-hour incubation in control medium alone (n = 9) as well as in control medium with L-type Ca^{2+} channel activator 10 μM (-)BayK8644 (n = 9), L-type Ca^{2+} channel inhibitor 10 μM nifedipine (n = 8), or T-type channel inhibitor 5 μM ML218 (n = 8) (mean ± SEM, cell lines 08/023 and 11/013, days post-confluence 66–147). *Statistically significant difference with $p < .05$. Abbreviation: VEGF, vascular endothelial growth factor.

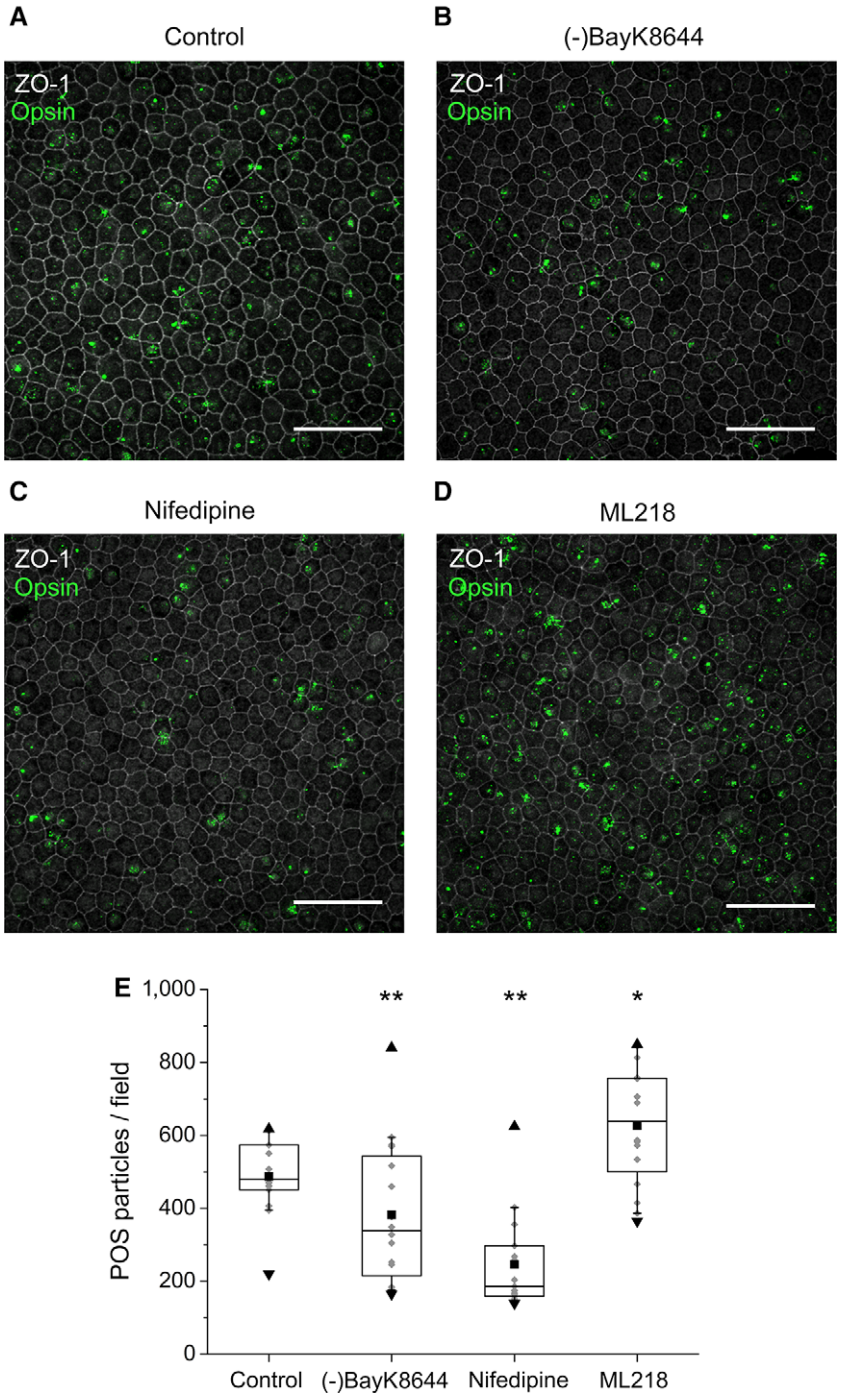

Figure 6. The effect of Ca_V channel modulators on POS phagocytosis in hESC-RPE. Mature hESC-RPE monolayers were incubated with purified porcine POSs in the pulse-chase phagocytosis assay. Xy-maximun intensity projections of the confocal images show both bound and internalized POS particles that were stained with opsin (green) together with the tight junction protein ZO-1 (gray) in **(A)** control conditions, and in the presence of Ca_V channel modulators **(B)** (-)BayK8644, **(C)** nifedipine, or **(D)** ML218. Scale bars 50 μm. **(E):** Quantification of POS particles in control conditions yielded the median value of 485 POS particles/field (n = 16). When modulating the Ca_V channels pharmacologically, the value changed in the presence of (-)BayK8644 to 339 POS particles/field (n = 15), nifedipine to 186 POS particles/field (n = 15), and ML218 to 639 POS particles/field (n = 16). The box limits 25%–75% of the gray data points; the whiskers include 10%–90% of the data; the center line shows the median value; the black square describes the mean; the black triangles present the minimum and the maximum values. Cell line 11/013, days post-confluence 147. Statistically significant differences with *p < .05 or **p < .001. Abbreviations: POS, photoreceptor outer segment; ZO-1, Zonula occludens.

showed that in mature hESC-RPE, $Ca_V1.3$ localized quite homogeneously on the apical and basolateral cell membranes. Intriguingly, in maturing hESC-RPE, $Ca_V1.3$ appeared as distinct foci that co-localized with PCNT to the base of the primary cilia. A similar punctuated appearance has been previously shown for TRP channel TRPM3 in human fetal RPE [94]. PCNT is

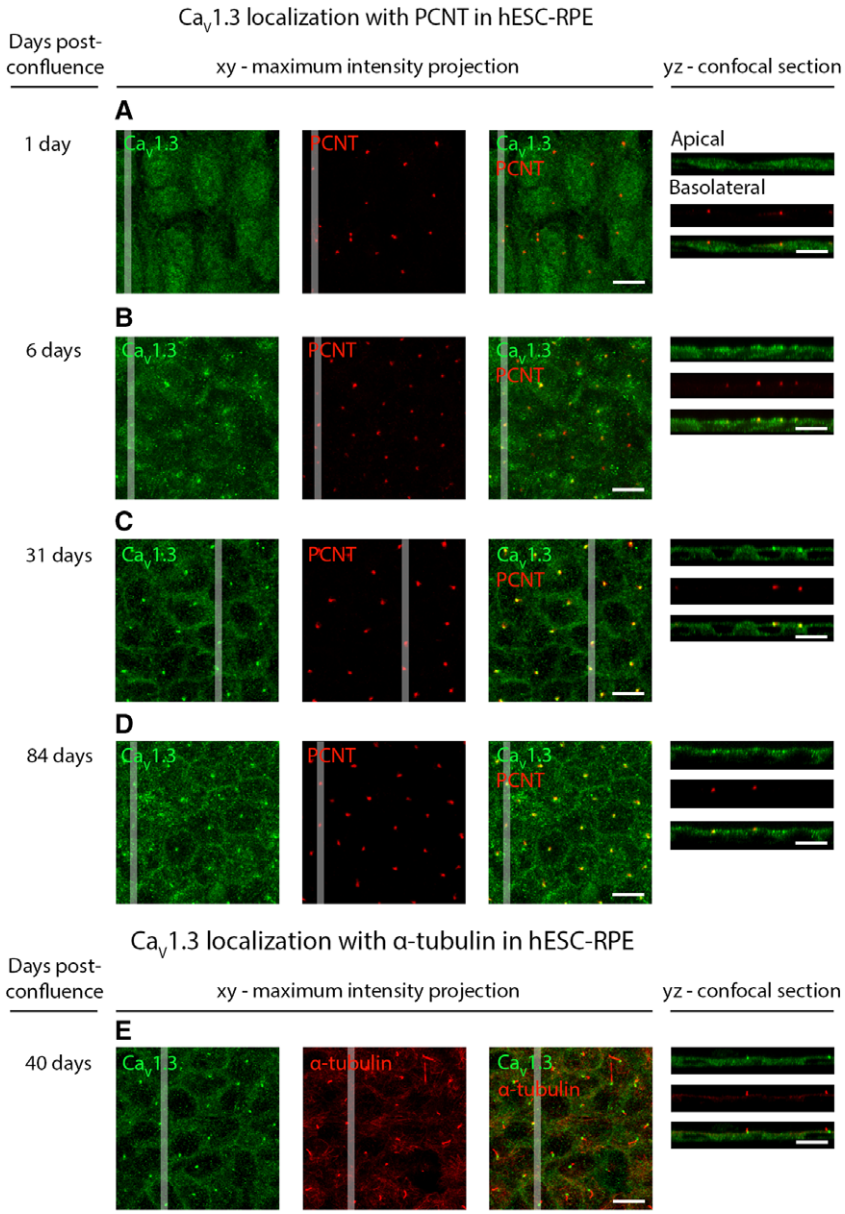

Figure 7. Localization of $Ca_V1.3$ during hESC-RPE maturation. Immunolabeling of $Ca_V1.3$ (green) together with centrosome protein PCNT (red) from post-confluence day 1 to post-confluence day 84 at four time points: **(A)** day 1, **(B)** day 6, **(C)** day 31, and **(D)** day 84 (cell line 08/017). **(E):** Labeling acetylated α-tubulin (red) together with $Ca_V1.3$ (green) shows the localization of $Ca_V1.3$ at the base of the primary cilia during maturation (cell line 08/017, days post-confluence 40). The confocal images are shown as xy-maximum intensity projections and yz-confocal sections (apical side upwards, localization of the section highlighted with a white bar). Scale bars 10 µm. Abbreviations: Ca_V, voltage-gated Ca^{2+} channel; hESC, human embryonic stem cell; RPE, retinal pigment epithelium; PCNT, pericentrin.

critical for the cilia formation, and relevant for our observations, PCNT is suggested to recruit protein complexes involved in cilia assembly and calcium signaling to the base of the primary cilia [66]. On the other hand, primary cilia has been shown to regulate L-type Ca^{2+} channel expression in mouse renal epithelial cells [95]. This occurs through Wnt signaling [95], and interestingly, recent work shows the importance of the regulation of Wnt signaling not only for RPE development [96] but also for RPE maturation [67]. Based on our data and taking into account these observations in the literature, it is possible, that $Ca_V1.3$ participates in ciliogenesis during RPE maturation or that its expression is coupled to the functioning of primary cilia in RPE maturation. This would not be surprising since primary cilia are important Ca^{2+} signaling organelles [97] with the expression of several different types of Ca^{2+} channels [98].

Conclusion

In this article, we demonstrate the presence of a functional machinery of voltage-gated Ca^{2+} channels in hESC-RPE, with L-type Ca^{2+} channel characteristics highly resembling the native RPE. We show a regulatory role for L-type Ca^{2+} channels in VEGF secretion and phagocytosis important for the

hESC-RPE functionality. We also provide novel information regarding the apical localization of $Ca_V1.3$ in RPE as well as its co-localization near the base of the primary cilia during hESC-RPE maturation. Our study represents an initial but significant progress toward a better understanding of Ca_V channels in stem cell-derived RPE, however, further studies are needed to elucidate the specific roles for T-type Ca^{2+} channels in RPE physiology. Overall, the results of the study are promising for the success of stem cell-based RPE transplantation therapies, but highlight the need for sufficient RPE maturation as a prerequisite for its fully functional Ca^{2+} machinery.

Acknowledgments

We thank Viivi Jokinen, Julia Johansson, Elina Hurskainen, Outi Heikkilä, Marja-Leena Koskinen, Outi Melin, Hanna Pekkanen, Outi Paloheimo, and Teemu Ihalainen for their technical assistance. The support from Tampere Imaging Facility and Tampere Facility of Electrophysiological Measurements is also greatly appreciated. This study was financially supported by the Academy of Finland (grant numbers 260375, 287287, 294054, 252225, 218050, 272808, 137801, 304909), the Emil Aaltonen Foundation, the Finnish Cultural Foundation, the Instrumentarium Science Foundation, the TEKES Human Spare Part Project and the Doctoral Programme of the President of Tampere University of Technology.

Author Contributions

I.V.: conception and design, collection and assembly of data, data analysis and interpretation, manuscript writing, final approval of manuscript; T.V.: collection and assembly of data, data analysis and interpretation, provision of study material, manuscript writing, final approval of manuscript; K.J.-U.: conception and design, collection and/or assembly of data, manuscript writing, final approval of manuscript; H.U.-J.: provision of study material, final approval of manuscript; H.S.: provision of study material, manuscript writing, final approval of manuscript; J.H.: financial support, manuscript writing, final approval of manuscript; S.N.: conception and design, financial support, collection and/or assembly of data, data analysis and interpretation, manuscript writing, final approval of manuscript.

Disclosure of Potential Conflicts of Interest

The authors indicated no potential conflicts of interest.

References

1 Strauss O. The retinal pigment epithelium in visual function. Physiol Rev 2005;85:845-881.

2 Wimmers S, Karl MO, Strauss O. Ion channels in the RPE. Prog Retin Eye Res 2007;26:263-301.

3 Ferrington DA, Sinha D, Kaarniranta K. Defects in retinal pigment epithelial cell proteolysis and the pathology associated with age-related macular degeneration. Prog Retin Eye Res 2016;51:69-89.

4 Wong WL, Su X, Li X et al. Global prevalence of age-related macular degeneration and disease burden projection for 2020 and 2040: A systematic review and meta-analysis. Lancet Glob Health 2014;2:e106-e116.

5 Riera M, Fontrodona L, Albert S et al. Comparative study of human embryonic stem cells (hESC) and human induced pluripotent stem cells (hiPSC) as a treatment for retinal dystrophies. Mol Ther Methods Clin Dev 2016;3:1-12.

6 Schwartz SD, Regillo CD, Lam BL et al. Human embryonic stem cell-derived retinal pigment epithelium in patients with age-related macular degeneration and Stargardt's macular dystrophy: Follow-up of two open-label phase 1/2 studies. Lancet 2015;385:509-516.

7 Song WK, Park K, Kim H et al. Treatment of macular degeneration using embryonic stem cell-derived retinal pigment epithelium: Preliminary results in Asian patients. Stem Cell Reports 2015;4:860-872.

8 Schwartz SD, Tan G, Hosseini H et al. Subretinal transplantation of embryonic stem cell–derived retinal pigment epithelium for the treatment of macular degeneration: An assessment at 4 years. Invest Ophthalmol Vis Sci 2016;57:ORSFc1-ORSFc9.

9 Mandai M, Watanabe A, Kurimoto Y et al. Autologous induced stem-cell–derived retinal cells for macular degeneration. N Engl J Med 2017;376:1038-1046.

10 Southwest Hospital, China. Clinical study of subretinal transplantation of human embryo stem cell derived retinal pigment epitheliums in treatment of macular degeneration diseases. Available at https://www.clinicaltrials.gov/ct2/show/NCT02749734. Accessed January 9, 2018.

11 Chinese Academy of Sciences. Subretinal transplantation of retinal pigment epitheliums in treatment of age-related macular degeneration diseases. Available at https://www.clinicaltrials.gov/ct2/show/NCT02755428. Accessed January 9, 2018.

12 Cell Cure Neurosciences Ltd. Safety and efficacy study of OpRegen for treatment of advanced dry-form age-related macular degeneration. Available at https://www.clinicaltrials.gov/ct2/show/NCT02286089. Accessed January 9, 2018.

13 Astellas Institute for Regenerative Medicine. Long term follow up of sub-retinal transplantation of hESC derived RPE cells in Stargardt macular dystrophy patients. Available at https://www.clinicaltrials.gov/ct2/show/NCT02445612. Accessed January 9, 2018.

14 Astellas Institute for Regenerative Medicine. Safety and tolerability of sub-retinal transplantation of hESC derived RPE (MA09-hRPE) cells in patients with advanced dry age related macular degeneration (Dry AMD). Available at https://www.clinicaltrials.gov/ct2/show/NCT01344993. Accessed January 9, 2018.

15 Astellas Institute for Regenerative Medicine. Sub-retinal transplantation of hESC derived RPE(MA09-hRPE)cells in patients with Stargardt's macular dystrophy. Available at https://www.clinicaltrials.gov/ct2/show/NCT01345006. Accessed January 9, 2018.

16 Astellas Institute for Regenerative Medicine. Long term follow up of sub-retinal transplantation of hESC derived RPE cells in patients with AMD. Available at https://www.clinicaltrials.gov/ct2/show/NCT02463344. Accessed January 9, 2018.

17 Pfizer. Retinal pigment epithelium safety study for patients in B4711001. Available at https://www.clinicaltrials.gov/ct2/show/NCT03102138. Accessed January 9, 2018.

18 Federal University of São Paulo. Stem cell therapy for outer retinal degenerations. Available at https://www.clinicaltrials.gov/ct2/show/NCT02903576. Accessed January 9, 2018.

19 Chinese Academy of Sciences. Treatment of dry age related macular degeneration disease with retinal pigment epithelium derived from human embryonic stem cells. Available at https://www.clinicaltrials.gov/ct2/show/NCT03046407. Accessed January 9, 2018.

20 Pfizer. A study of implantation of retinal pigment epithelium in subjects with acute wet age related macular degeneration. Available at https://www.clinicaltrials.gov/ct2/show/NCT01691261. Accessed January 9, 2018.

21 da Cruz L, Fynes K, Georgiadis O et al. Phase 1 clinical study of an embryonic stem cell–derived retinal pigment epithelium patch in age-related macular degeneration. Nat Biotechnol 2018;36:328-337.

22 Li Y, Tsai Y, Hsu C et al. Long-term safety and efficacy of human-induced pluripotent stem cell (iPS) grafts in a preclinical model of retinitis pigmentosa. Mol Med 2012;18:1312-1319.

23 Lu B, Malcuit C, Wang S et al. Long-term safety and function of RPE from human embryonic stem cells in preclinical models of macular degeneration. Stem Cells 2009;27: 2126-2135.

24 Kanemura H, Go MJ, Shikamura M et al. Tumorigenicity studies of induced pluripotent stem cell (iPSC)-derived retinal pigment epithelium (RPE) for the treatment of age-related macular degeneration. PLOS ONE 2014;9(1):e85336.

25 Koss MJ, Falabella P, Stefanini FR et al. Subretinal implantation of a monolayer of human embryonic stem cell-derived retinal pigment epithelium: A feasibility and safety study in Yucatan minipigs. Graefes Arch Clin Exp Ophthalmol 2016;254:1553-1565.

26 Galloway CA, Dalvi S, Hung SSC et al. Drusen in patient-derived hiPSC-RPE models of macular dystrophies. Proc Natl Acad Sci USA 2017;114:E8214-E8223.

27 Thomas BB, Zhu D, Zhang L et al. Survival and functionality of hESC-derived retinal pigment epithelium cells cultured as a monolayer on polymer substrates transplanted in RCS rats. Invest Ophthalmol Vis Sci 2016;57:2877-2887.

28 Carr A, Vugler AA, Hikita ST et al. Protective effects of human iPS-derived retinal pigment epithelium cell transplantation in the retinal dystrophic rat. PLOS ONE 2009;4(12):e8152.

29 Hongisto H, Jylhä A, Nättinen J et al. Comparative proteomic analysis of human embryonic stem cell-derived and primary human retinal pigment epithelium. Sci Rep 2017;7:6016.

30 Subrizi A, Hiidenmaa H, Ilmarinen T et al. Generation of hESC-derived retinal pigment epithelium on biopolymer coated polyimide membranes. Biomaterials 2012;33: 8047-8054.

31 Singh R, Shen W, Kuai D et al. iPS cell modeling of Best disease: Insights into the pathophysiology of an inherited macular degeneration. Hum Mol Genet 2013;22: 593-607.

32 Brandl C, Zimmermann SJ, Milenkovic VM et al. In-depth characterisation of retinal pigment epithelium (RPE) cells derived from human induced pluripotent stem cells (hiPSC). Neuromolecular Med 2014;16:551-564.

33 Kokkinaki M, Sahibzada N, Golestaneh N. Human iPS-derived retinal pigment epithelium (RPE) cells exhibit ion transport, membrane potential, polarized VEGF secretion and gene expression pattern similar to native RPE. Stem Cells 2011;29: 825-835.

34 Blenkinsop TA, Saini JS, Maminishkis A et al. Human adult retinal pigment epithelial stem cell–derived RPE monolayers exhibit key physiological characteristics of native tissue. Invest Ophthalmol Vis Sci 2015;56:7085-7099.

35 Maeda T, Lee MJ, Palczewska G et al. Retinal pigmented epithelial cells obtained from human induced pluripotent stem cells possess functional visual cycle enzymes in vitro and in vivo. J Biol Chem 2013;288:34484-34493.

36 Muñiz A, Greene WA, Plamper ML et al. Retinoid uptake, processing, and secretion in human iPS-RPE support the visual cycle. Invest Ophthalmol Vis Sci 2014;55: 198-209.

37 Peng S, Gan G, Qiu C et al. Engineering a blood-retinal barrier with human embryonic stem cell-derived retinal pigment epithelium: Transcriptome and functional analysis. Stem Cells Translational Medicine 2013;2:534-544.

38 Stanzel BV, Liu Z, Somboonthanakij S et al. Human RPE stem cells grown into polarized RPE monolayers on a polyester matrix are maintained after grafting into rabbit subretinal space. Stem Cell Reports 2014;2: 64-77.

39 Miyagishima KJ, Wan Q, Corneo B et al. In pursuit of authenticity: Induced pluripotent stem cell-derived retinal pigment epithelium for clinical applications. Stem Cells Translational Medicine 2016;5: 1562-1574.

40 Abu Khamidakh AE, Dos Santos FC, Skottman H et al. Semi-automatic method for Ca2+ imaging data analysis of maturing human embryonic stem cells-derived retinal pigment epithelium. Ann Biomed Eng 2016; 44:3408-3420.

41 Müller C, Más Gómez N, Ruth P et al. CaV1.3 L-type channels, maxiK Ca2 +-dependent K+ channels and bestrophin-1 regulate rhythmic photoreceptor outer segment phagocytosis by retinal pigment epithelial cells. Cell Signal 2014;26:968-978.

42 Wimmers S, Halsband C, Seyler S et al. Voltage-dependent Ca2+ channels, not ryanodine receptors, activate Ca2+-dependent BK potassium channels in human retinal pigment epithelial cells. Mol Vis 2008;14: 2340-2348.

43 Rosenthal R, Heimann H, Agostini H et al. Ca^{2+} channels in retinal pigment epithelial cells regulate vascular endothelial growth factor secretion rates in health and disease. Mol Vis 2007;13:443-456.

44 Rosenthal R, Malek G, Salomon N et al. The fibroblast growth factor receptors, FGFR-1 and FGFR-2, mediate two independent signalling pathways in human retinal pigment epithelial cells. Biochem Biophys Res Commun 2005;337:241-247.

45 Mergler S, Steinhausen K, Wiederholt M et al. Altered regulation of L-type channels by protein kinase C and protein tyrosine kinases as a pathophysiologic effect in retinal degeneration. FASEB J 1998; 12:1125-1134.

46 Wimmers S, Coeppicus L, Rosenthal R et al. Expression profile of voltage-dependent Ca2+ channel subunits in the human retinal pigment epithelium. Graefes Arch Clin Exp Ophthalmol 2008;246:685-692.

47 Ueda Y, Steinberg RH. Voltage-operated calcium channels in fresh and cultured rat retinal pigment epithelial cells. Invest Ophthalmol Vis Sci 1993;34: 3408-3418.

48 Ueda Y, Steinberg RH. Dihydropyridine-sensitive calcium currents in freshly isolated human and monkey retinal pigment epithelial cells. Invest Ophthalmol Vis Sci 1995;36:373-380.

49 Strauss O, Mergler S, Wiederholt M. Regulation of L-type calcium channels by protein tyrosine kinase and protein kinase C in cultured rat and human retinal pigment epithelial cells. FASEB J 1997;11:859-867.

50 Strauss O, Buss F, Rosenthal R et al. Activation of neuroendocrine L-type channels (α1D subunits) in retinal pigment epithelial cells and brain neurons by pp60c-src. Biochem Biophys Res Commun 2000;270:806-810.

51 Rosenthal R, Bakall B, Kinnick T et al. Expression of bestrophin-1, the product of the VMD2 gene, modulates voltage-dependent Ca2+ channels in retinal pigment epithelial cells. FASEB J 2006;20: 178-180.

52 Wollmann G, Lenzner S, Berger W et al. Voltage-dependent ion channels in the mouse RPE: Comparison with Norrie disease mice. Vision Res 2006;46:688-698.

53 Rosenthal R, Thieme H, Strauss O. Fibroblast growth factor receptor 2 (FGFR2) in brain neurons and retinal pigment epithelial cells act via stimulation of neuroendocrine L-type channels (Cav1.3). FASEB J 2001;15: 970-977.

54 Reichhart N, Markowski M, Ishiyama S et al. Rab27a GTPase modulates L-type Ca2+ channel function via interaction with the II–III linker of CaV1.3 subunit. Cell Signal 2015;27: 2231-2240.

55 Reichhart N, Milenkovic VM, Halsband C et al. Effect of bestrophin-1 on L-type Ca2+ channel activity depends on the Ca2+ channel beta-subunit. Exp Eye Res 2010;91:630-639.

56 Rohrer B, Kunchithapautham K, Genewsky A et al. Prolonged src kinase activation, a mechanism to turn transient, sublytic complement activation into a sustained pathological condition in retinal pigment epithelium cells. Adv Exp Med Biol 2014;801: 221-227.

57 Skottman H. Derivation and characterization of three new human embryonic stem cell lines in Finland. In Vitro Cell Dev Biol Anim 2010;46:206-209.

58 Vaajasaari H, Ilmarinen T, Juuti-Uusitalo K et al. Toward the defined and xeno-free differentiation of functional human pluripotent stem cell-derived retinal pigment epithelial cells. Mol Vis 2011;17: 558-575.

59 Bodenstein L, Sidman RL. Growth and development of the mouse retinal pigment epithelium: I. Cell and tissue morphometrics and topography of mitotic activity. Dev Biol 1987;121:192-204.

60 Johansson JK, Ihalainen TO, Skottman H et al. Fast voltage sensitivity in retinal pigment epithelium: Sodium channels and their novel role in phagocytosis. bioRxiv 2017;223719.

61 Schneider CA, Rasband WS, Eliceiri KW. NIH Image to ImageJ: 25 years of image analysis. Nat Methods 2012;9:671-675.

62 Mao Y, Finnemann SC. Analysis of photoreceptor outer segment phagocytosis by RPE cells in culture. Methods Mol Biol 2013; 935:285-295.

63 Luo Y, Zhuo Y, Fukuhara M et al. Effects of culture conditions on heterogeneity and the apical junctional complex of

the ARPE-19 cell line. Invest Ophthalmol Vis Sci 2006;47:3644-3655.

64 Karl MO, Kroeger W, Wimmers S et al. Endogenous Gas6 and Ca2+-channel activation modulate phagocytosis by retinal pigment epithelium. Cell Signal 2008;20: 1159-1168.

65 Burke JM. Epithelial phenotype and the RPE: Is the answer blowing in the Wnt? Prog Retin Eye Res 2008;27:579-595.

66 Jurczyk A, Gromley A, Redick S et al. Pericentrin forms a complex with intraflagellar transport proteins and polycystin-2 and is required for primary cilia assembly. J Cell Biol 2004;166:637-643.

67 May-Simera HL, Wan Q, Jha BS et al. Primary cilium-mediated retinal pigment epithelium maturation is disrupted in ciliopathy patient cells. Cell Rep 2018;22: 189-205.

68 Koschak A, Reimer D, Huber I et al. a1D (Cav1.3) subunits can form L-type Ca2+ channels activating at negative voltages. J Biol Chem 2001;276:22100-22106.

69 Singh A, Gebhart M, Fritsch R et al. Modulation of voltage- and Ca2 +-dependent gating of CaV1.3 L-type calcium channels by alternative splicing of a C-terminal regulatory domain. J Biol Chem 2008;283:20733-20744.

70 Striessnig J, Pinggera A, Kaur G et al. L-type Ca2+ channels in heart and brain. Wiley Interdiscip Rev Membr Transp Signal 2014;3:15-38.

71 Cordeiro S, Strauss O. Expression of Orai genes and ICRAC activation in the human retinal pigment epithelium. Graefes Arch Clin Exp Ophthalmol 2011;249:47-54.

72 Martínez-García MC, Martínez T, Pañeda C et al. Differential expression and localization of transient receptor potential vanilloid 1 in rabbit and human eyes. Histol Histopathol 2013;28:1507-1516.

73 Cordeiro S, Seyler S, Stindl J et al. Heat-sensitive TRPV channels in retinal pigment epithelial cells: Regulation of VEGF-A secretion. Invest Ophthalmol Vis Sci 2010;51: 6001-6008.

74 Wimmers S, Strauss O. Basal calcium entry in retinal pigment epithelial cells is mediated by TRPC channels. Invest Ophthalmol Vis Sci 2007;48:5767-5772.

75 Balse E, Steele DF, Abriel H et al. Dynamic of ion channel expression at the plasma membrane of cardiomyocytes. Physiol Rev 2012;92:1317-1358.

76 Perez-Reyes E. Molecular physiology of low-voltage-activated T-type calcium channels. Physiol Rev 2003;83:117-161.

77 Strauss O, Wienrich M. Ca2+—conductances in cultured rat retinal pigment epithelial cells. J Cell Physiol 1994;160:89-96.

78 Kovach JL, Schwartz SG, Flynn HW Jr et al. Anti-VEGF treatment strategies for wet AMD. J Ophthalmol 2012;2012:1-7.

79 Klettner A, Kaya L, Flach J et al. Basal and apical regulation of VEGF-A and placenta growth factor in the RPE/choroid and primary RPE. Mol Vis 2015;21:736-748.

80 Blaauwgeers HGT, Holtkamp GM, Rutten H et al. Polarized vascular endothelial growth factor secretion by human retinal pigment epithelium and localization of vascular endothelial growth factor receptors on the inner choriocapillaris: Evidence for a trophic paracrine relation. Am J Pathol 1999;155: 421-428.

81 Hollborn M, Vogler S, Reichenbach A et al. Regulation of the hyperosmotic induction of aquaporin 5 and VEGF in retinal pigment epithelial cells: Involvement of NFAT5. Mol Vis 2015;21:360-377.

82 Faby H, Hillenkamp J, Roider J et al. Hyperthermia-induced upregulation of vascular endothelial growth factor in retinal pigment epithelial cells is regulated by mitogen-activated protein kinases. Graefes Arch Clin Exp Ophthalmol 2014;252: 1737-1745.

83 Kannan R, Zhang N, Sreekumar PG et al. Stimulation of apical and basolateral vascular endothelial growth factor-A and vascular endothelial growth factor-C secretion by oxidative stress in polarized retinal pigment epithelial cells. Mol Vis 2006;12: 1649-1659.

84 Gal A, Li Y, Thompson DA et al. Mutations in MERTK, the human orthologue of the RCS rat retinal dystrophy gene, cause retinitis pigmentosa. Nat Genet 2000; 26:270-271.

85 Vollrath D, Yasumura D, Benchorin G et al. Tyro3 modulates mertk-associated retinal degeneration. PLoS Genet 2015;11: e1005723.

86 Hall MO, Abrams TA, Mittag TW. ROS ingestion by RPE cells is turned off by increased protein kinase C activity and by increased calcium. Exp Eye Res 1991;52: 591-598.

87 Milenkovic VM, Krejcova S, Reichhart N et al. Interaction of bestrophin-1 and Ca2+ channel β-subunits: Identification of new binding domains on the bestrophin-1 C-terminus. PLoS ONE 2011;6(4):e19364.

88 Szklarczyk D, Franceschini A, Wyder S et al. STRING v10: Protein-protein interaction networks, integrated over the tree of life. Nucleic Acids Res 2015;43:447-452.

89 Mazzoni F, Safa H, Finnemann SC. Understanding photoreceptor outer segment phagocytosis: Use and utility of RPE cells in culture. Exp Eye Res 2014;126:51-60.

90 Sugino IK, Sun Q, Wang J et al. Comparison of FRPE and human embryonic stem cell–derived RPE behavior on aged human Bruch's membrane. Invest Ophthalmol Vis Sci 2011;52:4979-4997.

91 Yang X, Chung JY, Rai U et al. Cadherins in the retinal pigment epithelium (RPE) revisited: P-cadherin is the highly dominant cadherin expressed in human and mouse RPE in vivo. PLoS ONE 2018;13(1):e0191279.

92 Bennis A, Gorgels TG, Ten Brink JB et al. Comparison of mouse and human retinal pigment epithelium gene expression profiles: Potential implications for age-related macular degeneration. PLoS ONE 2015;10(10):e0141597.

93 Bakall B, Marmorstein LY, Hoppe G et al. Expression and localization of bestrophin during normal mouse development. Invest Ophthalmol Vis Sci 2003;44:3622-3628.

94 Zhao PY, Gan G, Peng S et al. TRP channels localize to subdomains of the apical plasma membrane in human fetal retinal pigment epithelium. Invest Ophthalmol Vis Sci 2015;56:1916-1923.

95 Muntean BS, Jin X, Williams FE et al. Primary cilium regulates CaV1.2 expression through Wnt signaling. J Cell Physiol 2014;229:1926-1934.

96 Westenskow P, Piccolo S, Fuhrmann S. Beta-catenin controls differentiation of the retinal pigment epithelium in the mouse optic cup by regulating Mitf and Otx2 expression. Development 2009;136:2505-2510.

97 Delling M, DeCaen PG, Doerner JF et al. Primary cilia are specialized calcium signalling organelles. Nature 2013;504:311-314.

98 Pablo JL, DeCaen PG, Clapham DE. Progress in ciliary ion channel physiology. J Gen Physiol 2017;149:37-47.

See www.StemCellsTM.com for supporting information available online.